Research Article

Enhancing LVRT Capability of DFIG-Based Wind Turbine Systems with SMES Series in the Rotor Side

Xiao Zhou, Yuejin Tang, and Jing Shi

State Key Laboratory of Advanced Electromagnetic Engineering and Technology, R&D Center of Applied Superconductivity, Huazhong University of Science and Technology, Wuhan 430074, China

Correspondence should be addressed to Jing Shi; shijing@mail.hust.edu.cn

The necessary Low Voltage Ride Through (LVRT) capability is very important to wind turbines. This paper presents a method to enhance LVRT capability of doubly fed induction generators- (DFIGs-) based wind turbine systems with series superconducting magnetic energy storage (SMES) in the rotor side. When grid fault occurs, series SMES in the rotor side is utilized to produce a desired output voltage and absorbs energy. Compared with other methods which enhance LVRT capability with Superconducting Fault-Current Limiter-Magnetic Energy Storage System (SFCL-MESS), this strategy can control the output voltage of SMES to suppress the transient AC voltage component in the rotor directly, which is more effective and rapid. Theoretical study of the DFIG under low voltage fault is developed; the simulation results are operated by MATLAB/Simulink.

1. Introduction

Wind energy generation has experienced a fast development in the last two decades [1]. DFIG is the most widely used wind turbine, but it is vulnerable to low voltage fault. Many wind turbines trip off from the grid due to the lack of LVRT capability [2].

There are many enhanced ways to solve this problem. Crowbar is a commonly used protection method to implement the LVRT capability [3–5]; it can effectively suppress overvoltage and overcurrent but it needs to absorb a large amount of reactive power from the grid, which will do harm to the grid. Improving control strategy of grid converter or rotor converter has been studied by many researchers [6–8], but it cannot work effectively when deep voltage drop occurs. Energy storage device is suitable for dynamic matching of intermittent wind power. The use of supercapacitors or batteries for WTGs has been studied by some researchers [9–11]. SMES used in DFIGs to reduce power fluctuation and alleviate the influence on power quality has been studied in some papers [12]. The application of SFCL-SMES in the rotor side of the DFIG has been carried out. But it is connected with the DFIG through a three-phase diode rectifier; thus the SFCL-MES is inserted into rotor circuit as an impedance,

which will not provide help in enhancing the controllability of the RSC.

This paper presents a new method to enhance LVRT capability of DFIG with SMES. SMES, with its high efficiency and quick response ability to power compensation, could be a good choice for ESD in DFIG. Most studies applied ESD to solve the problem which are usually in parallel with the DC side. The proposed method in this paper is to generate a desired output voltage utilizing series SMES in the rotor side. Through the analysis of the rotor side voltage under low voltage fault, counter-electromotive force generated by SMES can counteract overvoltage and then overcurrent quickly and effectively. The mathematical model of DFIG will be illustrated first. Then, behavior of the DFIG in normal situation and under low voltage fault will be analyzed and the control strategy of VSC-SMES will be introduced.

2. Math Model of DFIG

The stator windings of the DFIG wind turbine are directly connected to the grid. The rotor winding is connected to the grid via back-to-back transformers, where the converter near the grid side is called grid sided converter (GSC) while

near the rotor side converter it is called rotor sided converter (RSC). The stator voltage is provided by the grid. The rotor voltage is provided by the back-to-back transformers, which can be adjusted in frequency, phase, and amplitude.

In this paper, the control system is implemented considering a stator voltage oriented (SVO) control philosophy in the d/q reference frame [13]. In this kind of systems, the d/q-axes are aligned with the stator voltage. Thus, the park model of the DFIG can be expressed as follows:

$$
\begin{aligned}
u_{dr} &= R_r i_{dr} + \frac{d\psi_{dr}}{dt} - (\omega_1 - \omega_r)\,\psi_{qr} \\[4pt]
u_{qr} &= R_r i_{qr} + \frac{d\psi_{qr}}{dt} + (\omega_1 - \omega_r)\,\psi_{dr} \\[4pt]
u_{ds} &= R_s i_{ds} + \frac{d\psi_{ds}}{dt} - \omega_1 \psi_{qs} \\[4pt]
u_{qs} &= R_s i_{qs} + \frac{d\psi_{qs}}{dt} + \omega_1 \psi_{ds} \\[4pt]
\psi_{ds} &= L_s i_{ds} + L_m i_{dr} \\[4pt]
\psi_{qs} &= L_s i_{qs} + L_m i_{qr} \\[4pt]
\psi_{dr} &= L_m i_{ds} + L_r i_{dr} \\[4pt]
\psi_{qr} &= L_m i_{qs} + L_r i_{qr},
\end{aligned}
\tag{1}
$$

where ψ is the magnetic flux, L is the inductances, u and i are voltage and current, respectively, R is the resistance, subscripts s, r, m represent the stator, rotor, and mutual, respectively, and ω_1 and ω_r are the synchronous and rotating angular frequencies ($\omega_s = \omega_1 - \omega_r$).

Once there is a grid fault, the stator voltage will change immediately because it is connected to the grid directly. But, according to the principle of flux conservation, the amplitude of stator flux will not transition. At the moment when the voltage drops, the stator flux linkage contains an AC component and a DC component, which will induce overvoltage in rotor side with different frequencies.

As analyzed in [14], the rotor back EMF voltage can be expressed as follows:

$$
\begin{aligned}
u_{rdq} &= j\frac{L_m}{L_s}\omega_s \psi_{s2dq} \\[4pt]
&\quad - j\frac{L_m}{L_s}\omega_r \left(\psi_{s0dq} - \psi_{s2dq}\right) e^{-\sigma t} e^{-j\omega_s t},
\end{aligned}
\tag{2}
$$

where ψ_{s0dq} and ψ_{s2dq} are normal-state stator flux and fault-state stator flux. The rotor back EMF voltage is mainly decided by part two of (2) because the slip frequency is much smaller than rotor frequency. And the second part in (2) is decided by the stator flux which can be several times the default value.

3. Methodology of DFIG and SMES Model

Unlike SFCL-MES, this paper controls the SMES output voltage through converter switch control, which could suppress the overvoltage in rotor side.
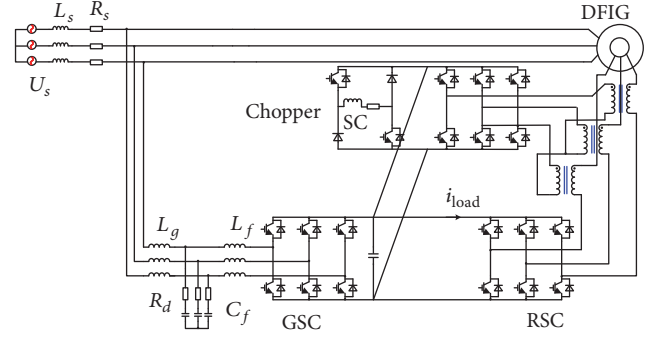
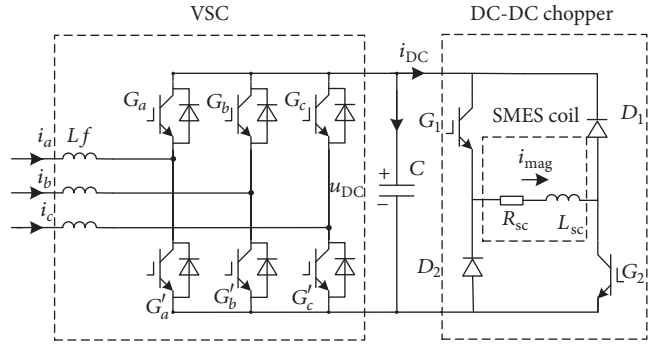

FIGURE 1: Topology of the whole system.
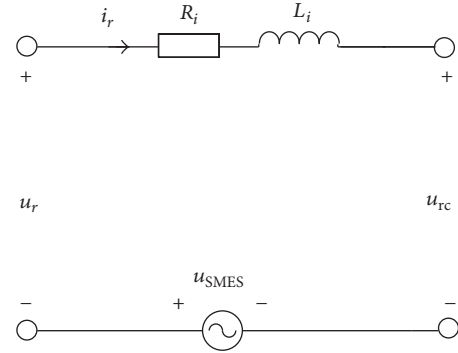

FIGURE 2: Topology of VSC-SMES.

FIGURE 3: Equivalent circuit of the series SMES.

The topology of the whole system is shown in Figure 1. SMES is connected to the rotor side by a Voltage Source Converter (VSC). Topology of VSC-SMES is given in Figure 2. SMES can exchange active and reactive power with the system quickly and independently [13].

In the case of normal power supply, SMES is in standby mode. In this case, the series SMES will introduce resistance and reactance to DFIG. Thus the rotor voltage will not equate to rotor converter voltage. As shown in Figure 3, R_i and L_i are the introduced resistance and reactance, respectively. In order to eliminate the influence of the rotor voltage by series SMES, the control of series SMES is to realize
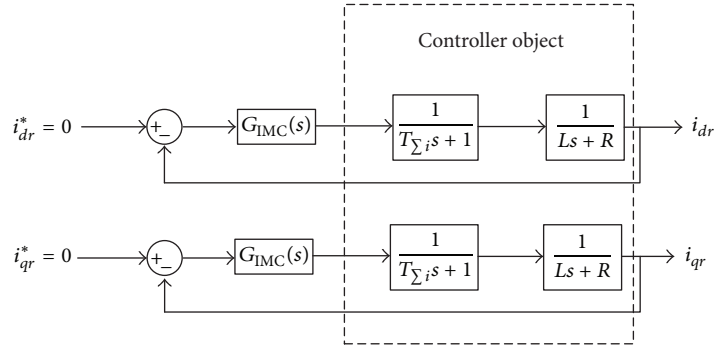
$$
u_r = u_{rc}.
\tag{3}
$$

FIGURE 4: The current inner loop control stratagem.

When low voltage fault occurs, the SMES outputs the voltage to suppress the rotor back EMF voltage induced by stator; thus the rotor current is supposed to be zero when fault occurs and the rotor back EMF voltage induced by stator u^*_r can be shown as follows:

$$u^*_{dr} = L_m \frac{di_{ds}}{dt}$$

$$u^*_{qr} = L_m \frac{di_{qs}}{dt}. \tag{4}$$

The stator current under grid fault after doing Laplace transform can be expressed as follows [15]:

$$i_{ds} = \frac{(L_s + R_s)\, u_{ds} + \omega_1 L_s u_{qs}}{(L_s^2 s^2 + 2L_s R_s s + R_s^2 + \omega_1^2 L_s^2)}$$
$$- \frac{(L_s s^2 + R_s s + \omega_1^2 L_s)\, L_m i_{dr} - R_s \omega_1 L_m i_{qr}}{(L_s^2 s^2 + 2L_s R_s s + R_s^2 + \omega_1^2 L_s^2)}$$

$$i_{qs} = \frac{(L_s + R_s)\, u_{qs} - \omega_s L_s u_{ds}}{(L_s^2 s^2 + 2L_s R_s s + R_s^2 + \omega_1^2 L_s^2)}$$
$$- \frac{(L_s s^2 + R_s s + \omega_1^2 L_s)\, L_m i_{qr} + R_s \omega_1 L_m i_{dr}}{(L_s^2 s^2 + 2L_s R_s s + R_s^2 + \omega_1^2 L_s^2)}. \tag{5}$$

Considering that $R_s^2, R_s \omega_s L_m$ are approximately 0, the equation can be simplified as:

$$i_{ds} = \frac{1}{L_s^2} \frac{L_s s + R_s}{s^2 + 2(R_s/L_s) + \omega_1^2} \cdot u_{ds} - \frac{L_m}{L_s} \cdot i_{dr}$$

$$i_{qs} = \frac{1}{L_s^2} \frac{(-L_s \omega_1)}{s^2 + 2(R_s/L_s) + \omega_1^2} \cdot u_{ds} - \frac{L_m}{L_s} \cdot i_{qr}. \tag{6}$$

According to the above analysis, if the rotor side converter could provide relative excitation voltage to u^*_r, the low LVRT capability of DFIG will be enhanced. Thus set u^*_r as the reference voltage of VSC-SMES under grid fault. The VSC-SMES reference voltage calculation process is presented in Figure 5.

3.1. SMES Control

3.1.1. VSC Control. As shown in Figure 2, through the park transformation, the mathematical model of VSC in the dq reference frame is expressed as follows:

$$L \frac{di_d}{dt} = -R i_d + \omega L i_q + u_{sd} - u_{DC} s_d$$

$$L \frac{di_q}{dt} = -R i_q - \omega L i_d + u_{sq} - u_{DC} s_q \tag{7}$$

$$C \frac{du_{DC}}{dt} = \frac{3}{2} (i_q s_q + i_d s_d) - i_{chopper}.$$

The current inner loop control of VSC adopts the internal model control strategy [14]; the control block diagram is shown in Figure 4. The closed-loop transfer function of the current inner loop is

$$W_{ci}(s) = \frac{1}{T_f^2 s^2 + 2\xi T_f s + 1}. \tag{8}$$

For achieving the purpose of rapid response of the current inner loop, let T_f be equal to 0.0002 s.

3.1.2. DC-DC Chopper Control. Chopper has two basic modes of operation: (1) magnetizing mode; (2) releasing magnetic mode. The mathematical model of chopper is

$$L_{sc} \frac{di_{mag}}{dt} = -R_{sc} i_{mag} + (D_1 + D_2 - 1) u_{DC}$$

$$C \frac{du_{DC}}{dt} = -(D_1 + D_2 - 1) i_{mag} + i_{DC}, \tag{9}$$

where i_{mag} is the current of magnet and D is the switch state of each switch; if switch 1 is on, D_1 is equal to 1.

In normal operation, the control of chopper is to limit the magnet current in a setting scale. When low voltage fault happens, the control of chopper is to maintain the stability of the DC voltage. The control strategy of SMES is shown in Figure 5.

3.2. RSC Control. In normal operation, the control of d/q component of rotor current is to control the active and
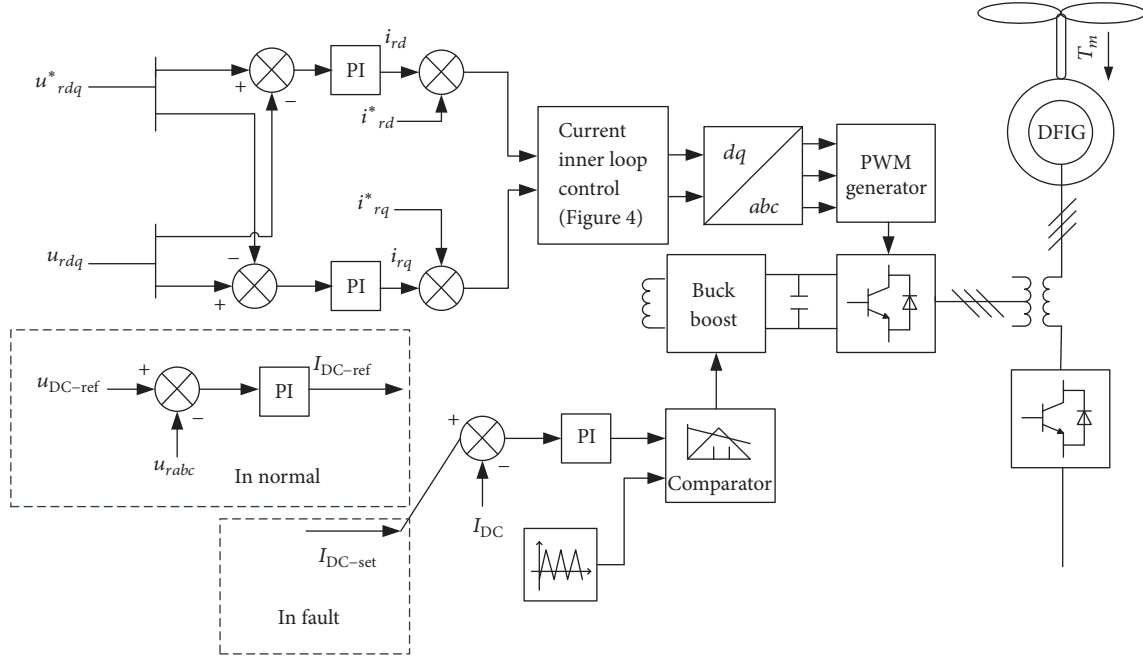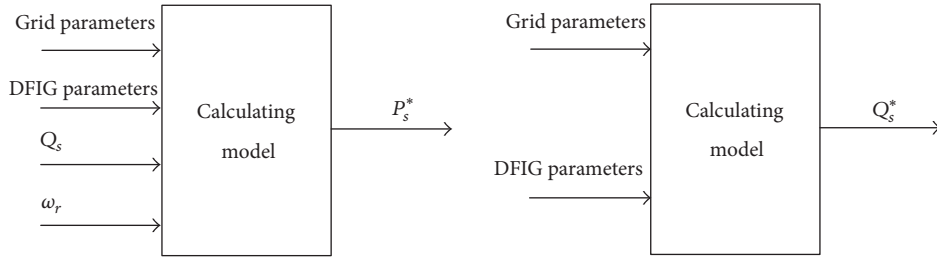
FIGURE 5: The control stratagem for SMES.

FIGURE 6: Reference power calculation model of DFIG.

reactive power of DFIG. Generally, the purpose of control system is to obtain the max wind power.

The essence of the maximum wind energy tracking is to control the DFIG output active power and control electromagnetic torque to achieve the best speed control. When the mechanical output of the wind turbine achieves maximum output power, the reference active power of DFIG P_s^* is equal to stator power P_s, as shown as follows:

$$P_s^* = \frac{1}{1-s}\left(P_{\max} - P_{\mathrm{ms}}\right) - P_{\mathrm{cus}}, \tag{10}$$

where P_{ms} is the mechanical loss of wind turbine and P_{cus} is the copper loss of stator, which is related to I_s and R_s. After doing identity transformation, (9) can be expressed as follows:

$$A\left(P_s^*\right)^2 + BP_s^* + C = 0$$

$$A = \frac{R_s}{3U_s^2}, \quad B = 1, \quad C = \frac{1}{s-1}\left(k_w\omega_w^3 - P_{ms}\right) + \frac{R_s}{3U_s^2}Q_s. \tag{11}$$

The reactive reference power value Q_s^* can be calculated by achieving the lowest loss of DFIG or improving the system's ability to regulate power. In this paper, Q_s^* is calculated to achieve the lowest loss of DFIG. Thus the expression of Q_s^* is shown as follows:

$$Q_s^* = -\frac{3X_s R_r U_s^2}{R_s X_m^2 + R_r R_s^2 + R_r X_s^2}. \tag{12}$$

The reference power calculation model of DFIG is shown in Figure 6.

When a fault occurs, the control strategy of rotor converter is irrelevant. Considering SMES will absorb the wind energy, i^*_{dr} and i^*_{qr} can be set to zero to prevent the energy through the converter. Thus, the capacitor in DC side will not absorb a lot of energy and its voltage will not increase sharply. The control stratagem of RSC, in normal situation and when voltage drop happens, is shown in Figure 7.

3.3. GSC Control. The purpose of GSC control is to maintain DC capacitor voltage stability and control the factor of input
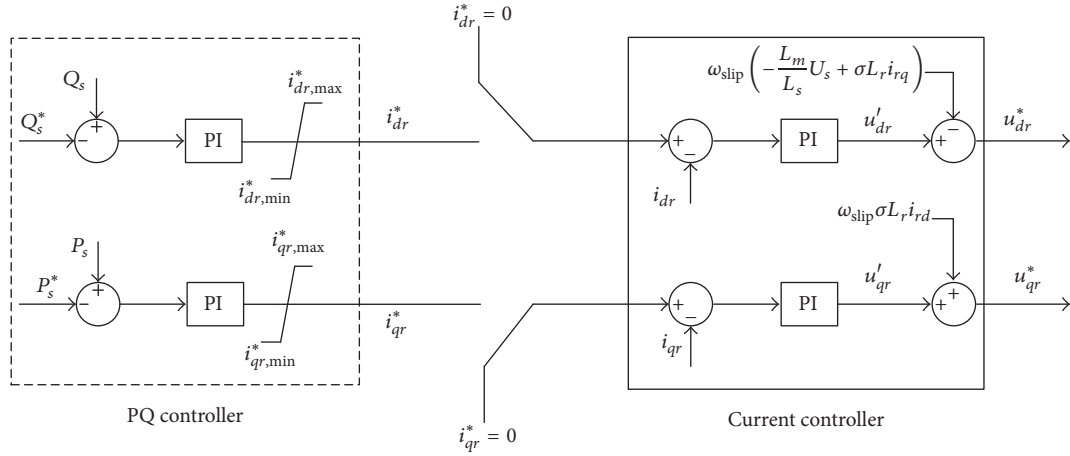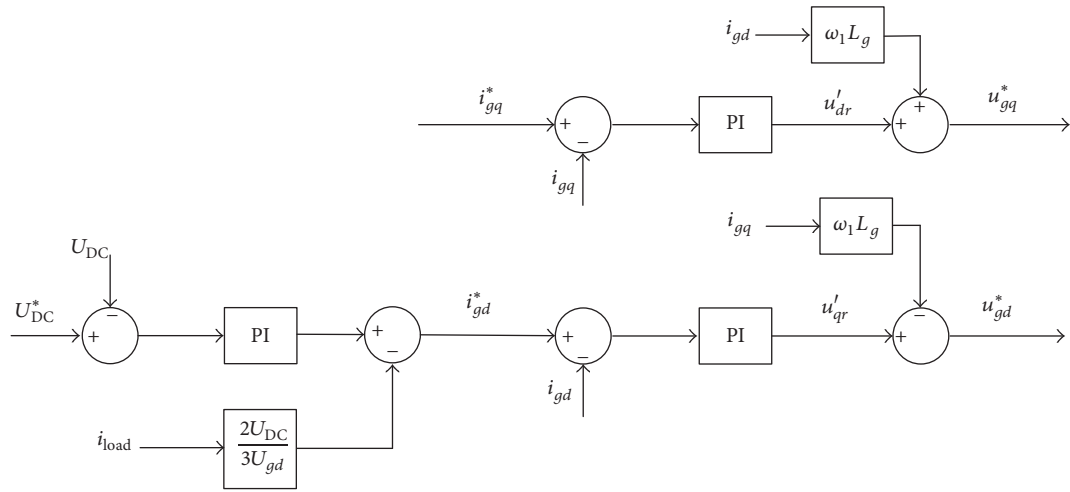
FIGURE 7: Control block diagram of the RSC.

FIGURE 8: Control block diagram of the GSC.

power. The GSC control system is divided into two parts: the outer voltage loop and the inner current loop, which is shown in Figure 8. Compensation of load disturbances is achieved by feedforward of the load current i_{load}. System is decoupled by introduced current state feedback $w_1 L_g i_{gd}$, $w_1 L_g i_{gq}$.

4. Economic Analysis

Compared to other energy storage devices, SEMS has the advantage of high response speed, high efficiency, high-power density, and high cycle life characteristics. But the application of SMES in DFIG will increase the cost of the system. Therefore, the capital cost of SMES applied in DFIG is an indispensable part of DFIG's technical performance. In terms of energy storage devices, the capital costs contain energy cost \$/kWh, power cost \$/kW, and cycle cost. As the energy storage device is used in DFIG, high-power characteristic is necessary. The power costs of SMES are less

than their energy costs, and this is an indication that they are suitable for high-power applications. Table 1 shows the cost comparison for the storage technologies [16]. As can be seen from the table, SMES has a lower power cost compared to pumped-hydro storage, lithium-ion batteries and other energy storage devices. In addition, the long life of SMES makes it possible to participate in the protection of the entire life of the DFIG. In general, considering the economic and other technical performances, SMES is a good choice for ESD in DFIG.

5. Simulation Analysis and Conclusion

The simulations are carried out in MATLAB/Simulink. The simulation parameters are shown in Table 2. The simulation parameters of SMES are shown in Table 3. The purpose of the simulation is to observe the performance of the back-to-back converter when the grid fault occurs.
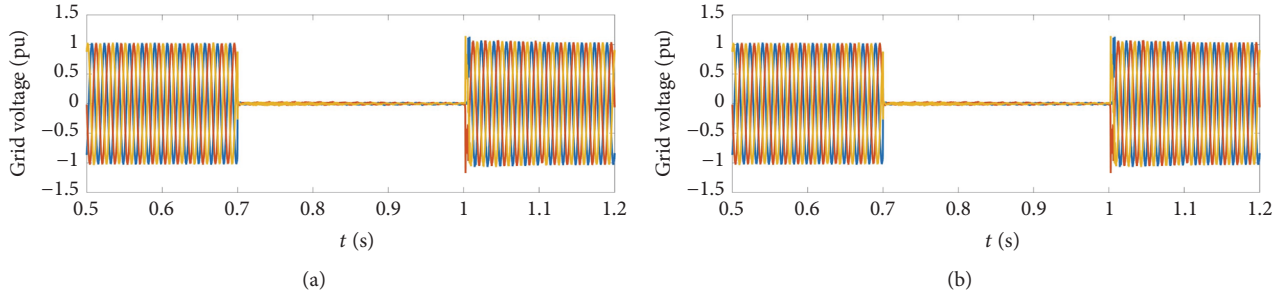
(a)

(b)

FIGURE 9: The grid voltage.

TABLE 1: Cost comparison for the storage technologies.

ESD	Capacity	Life	Power cost ($/kW)	Energy cost ($/kWh)
Pumped-hydro storage	100–2000 MW	>20 years	2000–4300	10–100
Compressed-air energy storage	100–300 MW	>20 years	400–1000	2–50
Flywheel energy storage	5 kW–1.5 MW	>15 years	250–350	1000–10000
Lithium-ion batteries	1–1000 kW	3000 cycles	1000–3000	1000–3800
Supercapacitors	1–100 kW	>50000 cycles	100–300	300–2000
Superconducting magnetic energy storage	10–500 kW	>20 years	200–400	500–1000
Vanadium redox battery	<10 MW	10–30 years	600–1500	150–1000

TABLE 2: DFIG parameters.

Symbol	Name	Quantity
S_N	Capacity	1.5 MW
f_N	System frequency	60 Hz
R_s	Stator resistance	0.016 p.u.
L_{ls}	Stator leakage inductance	0.16 p.u.
R_r	Rotor resistance	0.016 p.u.
L_{lr}	Rotor leakage inductance	0.16 p.u.
L_m	Magnetizing inductance	2.9 p.u
S_b	Base capacity	1.5/0.9 MVA
f_b	Base frequency	60 Hz
V_{s_nom}	Base stator voltage (V_{rms})	575 V
V_{r_nom}	Base rotor voltage (V_{rms})	1975 V

TABLE 3: SMES parameters.

Parameter	Value
HTS material	Bi 2223
Capacity	40 kJ/600 kW
Magnet inductance (L)	0.5 H
Magnet resistance	$2 \times 10^{-5}\ \Omega$
Filter capacitance (C)	0.02 F
Series transformer ratio	1
Transformer resistance	$1 \times 10^{-4}\ \Omega$

The transient grid voltage fault occurs at 0.7 s and lasts for 300 ms. The grid voltage during fault drops to 0. The grid voltage is shown in Figure 9. Figures 10 and 11 compare the currents of stator converter and rotor converter with and without SMES. When there is no SMES, in the moment of low voltage faults, the overcurrent of the stator and rotor side converters is almost five times larger than the normal operating range. With the proposed method, the currents of back-to-back converters are always in the affordable range. Moreover, as shown in Figure 13, the DC capacitor voltage is well suppressed during the fault. The output voltage of SMES in d/q frame is shown in Figure 12. The base voltage is the same as base rotor voltage. Figure 14 shows the transient SMES current response.

Compared to traditional control stratagems, the new control strategy with SMES can suppress the overcurrent in stator and rotor within the affordable range even when grid voltage drops to 0. The DC bus voltage can also be limited effectively.

This paper presents a new control stratagem to enhance the LVRT capability of DFIG with series SMES. By controlling the SMES output voltage with the proposed controller,

(a) The current of stator converter with SMES

(b) The current of stator converter without SMES

FIGURE 10

(a) The current of rotor converter with SMES

(b) The current of rotor converter without SMES

FIGURE 11

(a)

(b)
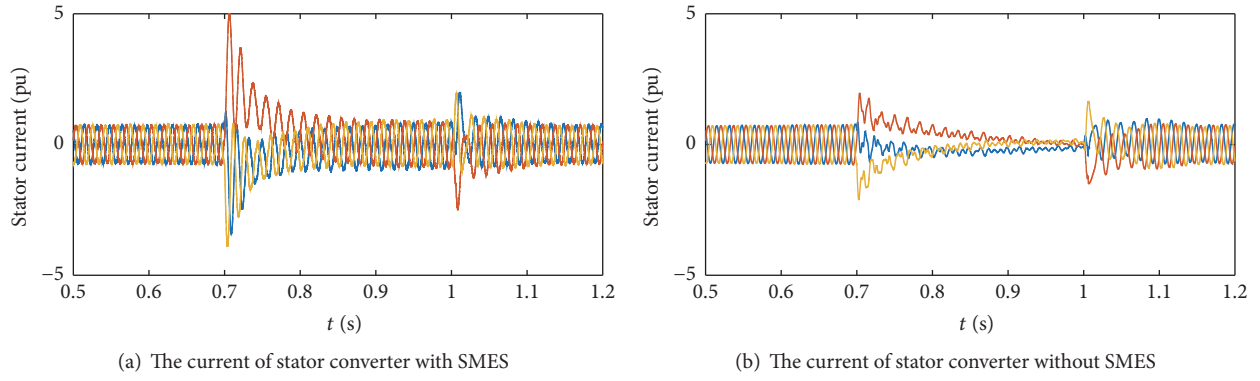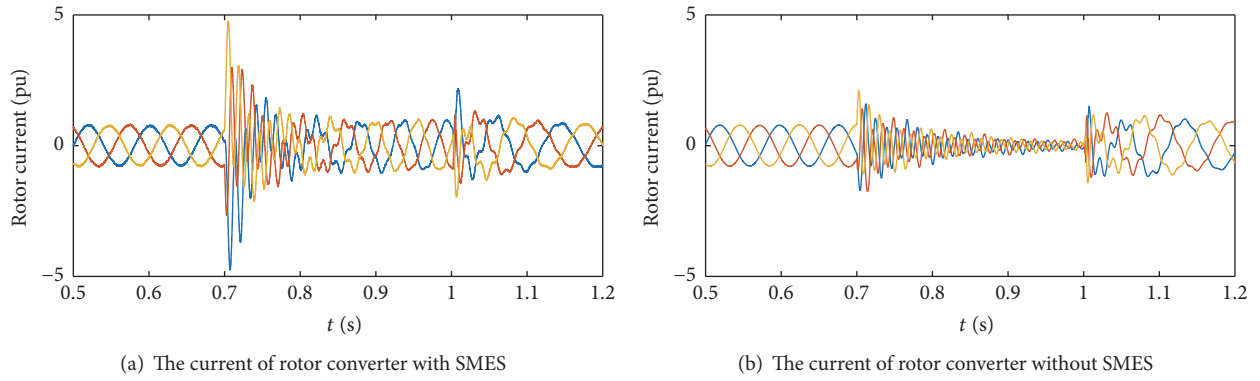
FIGURE 12: The SMES output voltage.

—— Without SMES
—— With SMES

FIGURE 13: The DC voltage.

Figure 14: The magnet current of SMES.

the converter currents and capacitor voltage in fault are suppressed effectively. The method has been validated by simulations in MATLAB/Simulink.
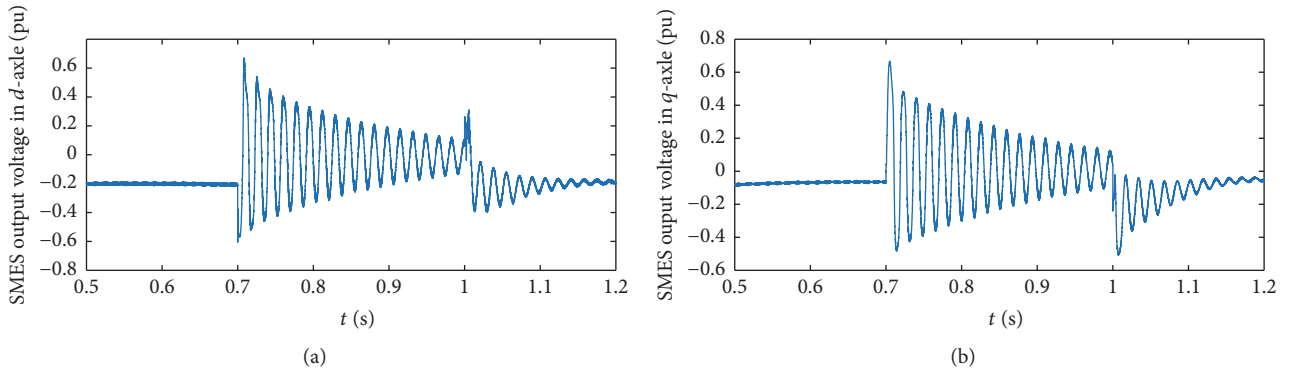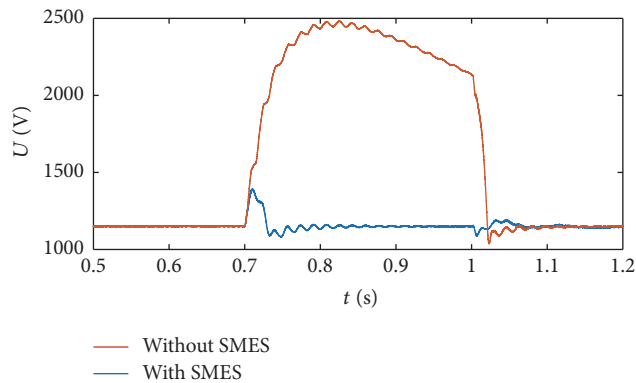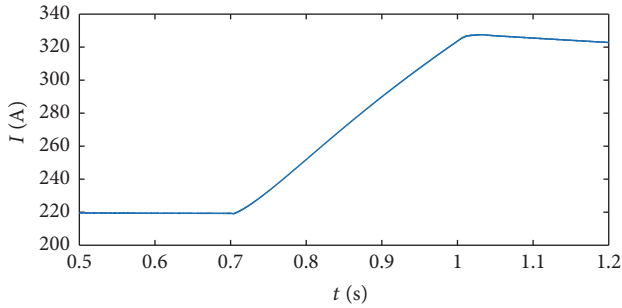
Conflicts of Interest

There are no conflicts of interest regarding the publication of this paper.

References

[1] Y.-W. Shen, D.-P. Ke, W. Qiao, Y.-Z. Sun, D. S. Kirschen, and C. Wei, "Transient reconfiguration and coordinated control for power converters to enhance the LVRT of a DFIG wind turbine with an energy storage device," *IEEE Transactions on Energy Conversion*, vol. 30, no. 4, pp. 1679–1690, 2015.

[2] J. Liu, H. Zhang, B. Yang, and Y. Min, "Fault ride through under unbalanced voltage sag of wind energy conversion system using superconducting magnetic energy storage," in *Proceedings of the 2nd IEEE International Future Energy Electronics Conference*, Taipei, Taiwan, November 2015.

[3] J. Niiranen, "Voltage dip ride through of a doubly-fed generator equipped with an active crowbar," in *Proceedings of the Nordic Wind Power Conference Nwpc*, 2004.

[4] L.-L. Sun, P. Yang, and Y. Wang, "Simulation research for LVRT of DFIG based on rotor active crowbar protection," in *Proceedings of the International Conference on Sustainable Power Generation and Supply, SUPERGEN 2012*, pp. 1–7, Hangzhou, China, September 2012.

[5] P. Su and K.-S. Zhang, "Simulation research for LVRT of DFIG with active IGBT Crowbar," *Power System Protection and Control*, vol. 38, no. 23, pp. 164–171, 2010.

[6] J. Hu, H. Wang, Y. He, and L. Xu, "Improved rotor current control of wind turbine driven doubly fed induction generators during network unbalance," in *Proceedings of the 1st International Conference on Sustainable Power Generation and Supply, SUPERGEN '09*, pp. 1–7, Nanjing, China, April 2009.

[7] T. K. A. Brekken and N. Mohan, "Control of a doubly fed induction wind generator under unbalanced grid voltage conditions," *IEEE Transactions on Energy Conversion*, vol. 22, no. 1, pp. 129–135, 2007.

[8] A. G. Abo-Khalil, D.-C. Lee, and J.-I. Jang, "Control of back-to-back PWM converters for DFIG wind turbine systems under unbalanced grid voltage," in *Proceedings of the 2007 IEEE International Symposium on Industrial Electronics, ISIE 2007*, pp. 2637–2642, Vigo, Spain, June 2007.

[9] C. Abbey and G. Joos, "Supercapacitor energy storage for wind energy applications," *IEEE Transactions on Industry Applications*, vol. 43, no. 3, pp. 763–776, 2007.

[10] B. S. Borowy and Z. M. Salameh, "Dynamic response of a stand-alone wind energy conversion system with battery energy storage to a wind gust," *IEEE Transactions on Energy Conversion*, vol. 12, no. 1, pp. 73–78, 1997.

[11] A. Yazdani, "Islanded operation of a doubly-fed induction generator (DFIG) wind-power system with integrated energy storage," in *Proceedings of the 2007 IEEE Canada Electrical Power Conference, EPC 2007*, pp. 153–159, Montreal, Canada, October 2007.

[12] J. Shi, Y. Tang, Y. Xia, L. Ren, and J. Li, "SMES based excitation system for doubly-fed induction generator in wind power application," *IEEE Transactions on Applied Superconductivity*, vol. 21, no. 3, pp. 1105–1108, 2011.

[13] Y. Zhang, Y. Tang, J. Li, J. Shi, and L. Ren, "Superconducting magnet based VSC suitable for interface of renewable power sources," *IEEE Transactions on Applied Superconductivity*, vol. 20, no. 3, pp. 880–883, 2010.

[14] W. Guo, L. Xiao, and S. Dai, "Enhancing low-voltage ride-through capability and smoothing output power of DFIG with a superconducting fault-current limiter-magnetic energy storage system," *IEEE Transactions on Energy Conversion*, vol. 27, no. 2, pp. 277–295, 2012.

[15] F. K. A. Lima, A. Luna, P. Rodriguez, E. H. Watanabe, and F. Blaabjerg, "Rotor voltage dynamics in the doubly fed induction generator during grid faults," *IEEE Transactions on Power Electronics*, vol. 25, no. 1, pp. 118–130, 2010.

[16] D. O. Akinyele and R. K. Rayudu, "Review of energy storage technologies for sustainable power networks," *Sustainable Energy Technologies and Assessments*, vol. 8, pp. 74–91, 2014.

Journal of
Engineering

The Scientific
World Journal

International Journal of
Rotating
Machinery

Journal of
Sensors

International Journal of
Distributed
Sensor Networks

Advances in
Civil Engineering

Journal of
Control Science
and Engineering

Journal of
Robotics

Journal of
Electrical and Computer
Engineering

Hindawi

Submit your manuscripts at
https://www.hindawi.com

Advances in
OptoElectronics

VLSI Design

International Journal of
Navigation and
Observation

Modelling &
Simulation
in Engineering

International Journal of
Aerospace
Engineering

International Journal of
Chemical Engineering

International Journal of
Antennas and
Propagation

Active and Passive
Electronic Components

Shock and Vibration

Advances in
Acoustics and Vibration